Oxygen Reduction Catalysts for Polymer Electrolyte Fuel Cells from the Pyrolysis of Iron Acetate Adsorbed on Various Carbon Supports

Frédéric Jaouen,[†,‡] Sébastien Marcotte,[†] Jean-Pol Dodelet,[*,†] and Göran Lindbergh[‡]

INRS-Énergie et Matériaux, C.P.1020, Varennes, Québec, Canada J3X 1S2, and Department of Chemical Engineering and Technology, Applied Electrochemistry, The Royal Institute of Technology (KTH), SE-100 44 Stockholm, Sweden

Received: July 16, 2002; In Final Form: October 18, 2002

Nonnoble metal catalysts for the electrochemical reduction of oxygen in acidic medium have been produced by adsorbing iron(II) acetate on 19 carbon supports. These materials were then pyrolyzed in an atmosphere containing NH_3. The 19 carbon supports are (i) six as-received commercial supports (Printex XE-2, Norit SX Ultra, Ketjenblack EC-600JD, acetylene black, Vulcan XC-72R, and Black Pearls 2000), (ii) three as-received developmental supports (Lonza HS300 and Sid Richardson RC1 and RC2), (iii) the same nine previous supports prepyrolyzed at 900 °C in an atmosphere containing NH_3 to increase their N content, and (iv) a synthetic carbon made by pyrolyzing perylene tetracarboxylic dianhydride at 900 °C in an atmosphere containing NH_3. The goal of this study is to determine the effect of the carbon support on the catalytic activity of the catalysts. The specific surface area, the pore size distribution, the N and O contents, and the electrocatalytic activities of the 19 types of catalysts were measured. It was found that the activity of the catalysts varies greatly from one carbon support to another, but neither the specific surface area of the catalysts nor the distribution of their macro- or mesopores is a determining factor for the catalytic activity. The most important factor is the N content of the materials; the higher it is, the higher is the density of the catalytic sites on their surface and the better is the electrocatalyst. Carbon supports that are devoid of N, however, display some lower catalytic activity, which is attributed to an iron oxide. The latter catalytic site occurs also in the other N-containing catalysts. In these materials there are, therefore, three catalytic sites at work: an iron oxide site and two N-containing sites labeled FeN_4/C and FeN_2/C, with the last site being the most active for oxygen electroreduction.

Introduction

Proton exchange membrane (PEM) fuel cells are electrical power generators. Among other fuel cell types, they are the best choice for a wide range of portable, stationary, and transportation applications because of their high power density and their relatively low temperature (∼80 °C) of operation. At this low temperature, catalysts are necessary to obtain useful current densities. However, only Pt and its alloys have been used to date in full-size applications at the anode and cathode because nonnoble metals corrode in the acidic environment (pH = 1) of the fuel cell membrane.[1] To achieve the lowest Pt loadings, the metal is supported on high-surface-area carbon blacks with high mesoporous areas (>75 m^2/g) and a degree of graphitic character, which leads to high electrical conductivity and good corrosion resistance, especially under cathodic conditions.[2] Pt remains, however, an expensive metal of low abundance, and hence, finding a nonnoble metal alternative is of interest. This will be difficult at the anode, but it might be possible at the cathode, provided that the alternative catalyst displays activity and stability approaching that of Pt. N_4−metal macrocycles are of interest in this respect. It has, indeed, been known for several years that Fe (or Co) tetraazaannulenes, porphyrins, and phthalocyanines and other N_4−Fe (or Co) chelates adsorbed onto carbon and heat-treated at various temperatures are catalysts for the reduction of O_2 in acidic medium.[3−30] The best electrocatalytic activities obtained with these precursors were shown for pyrolysis in the temperature range between 500 and 700 °C. In that temperature range, it has been proposed that the catalytic site is FeN_4/C (or CoN_4/C), where C represents the carbon support.[12,31] This site has been named the low-temperature catalytic site.[32] Another interesting catalytic site, labeled the high-temperature catalytic site,[32] has also been detected at pyrolysis temperatures ≥800 °C.[32−45] The complete structure of this second site is not yet known. However, some information about its formation and its composition has been collected. So far, the following facts are known:

(i) C, N, and Fe (or Co) are necessary to obtain that catalytic site. C is, in principle, any carbon support (carbon black, activated carbon, etc.). A carbon precursor can also be used, such as polyacrylonitrile (PAN[34]) or perylene tetracarboxylic dianhydride (PTCDA; see Figure 1 in ref 46).[32,46,47] The precursor of N might be either NH_3,[32,46,47] or CH_3CN[39,44] or N-containing molecules such as N_4−M macrocycles. The precursor of Fe (or Co) might be either an Fe (or Co) macrocycle, an Fe complex,[45] or even an Fe (or Co) salt as in refs 34, 44, and 46.

(ii) From XPS experiments on Fe-based catalysts,[46,47] it is known that, to obtain a catalyst, the nitrogen atoms on the carbon support have to be of the pyridinic type (N contributing one π electron to the conjugation of the graphene plane of the carbon support and having two other electrons in an *n* orbital).

* To whom all correspondence should be sent. E-mail: dodelet@inrs-ener.uquebec.ca.
† INRS-Énergie et Matériaux.
‡ The Royal Institute of Technology (KTH).

10.1021/jp021634q CCC: $25.00
Published on Web 01/21/2003

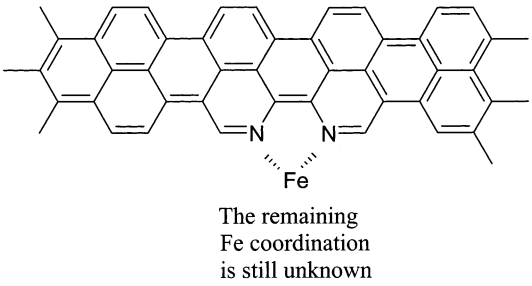

Figure 1. Proposed moiety of the FeN_2/C catalytic site.

(iii) From time-of-flight secondary ion mass spectrometry (ToF SIMS) on Fe-based catalysts,[32] it is also known that the pyridinic-type nitrogens have to be in a structure of the phenanthroline type to be able to coordinate the Fe ion in the catalytic site. Figure 1 shows what we know presently about the actual structure of the high-temperature catalytic site that we will represent as FeN_2/C. When such nitrogen atoms exist on the carbon support, adding Fe ions (even 50 ppm) induces catalytic activity. Increasing the Fe content increases the concentration of the catalytic sites until all nitrogens of the phenanthroline type are coordinated with Fe. This site saturation occurs at around 0.5 wt % Fe when iron(II) acetate is used as Fe precursor[46] and around 2 wt % Fe when a porphyrin-like chlorine−iron tetramethoxyphenyl porphyrin (Cl−FeTMPP) is used as Fe precursor.[32] Increasing the Fe content further produces Fe metal (and/or carbide) particles that induce graphitization around them.[48] These particles are catalytically inactive.[37]

Recent ToF SIMS experiments[49] made on catalysts prepared with low levels of Fe (0.2 wt %) provided by iron(II) acetate or also by ClFeTMPP as Fe precursors indicated that it was incorrect to talk about FeN_4/C and FeN_2/C as low- and high-temperature catalytic sites, respectively, because both sites were detected simultaneously at all pyrolysis temperatures and for both of these Fe precursors. Furthermore, the comparison of electrocatalytic activities and relative ToF SIMS intensities of specific ions that are characteristic of each catalytic sites indicated that FeN_2/C is, by far, the most active of the sites at all pyrolysis temperatures and for both Fe precursors.

Until now, we have not considered the nature of the carbon support as an important factor in the preparation of the Fe (or Co) -based catalysts. In our earlier experiments, we chose Vulcan XC-72R because it is a common support used for Pt-based catalysts. Then, to obtain ToF SIMS information and to be able to finely tune the metallic content of the catalysts, we switched to a synthetic carbon made by the pyrolysis of purified perylene tetracarboxylic dianhydride (PTCDA). Now it is important to determine whether the choice of a particular carbon support is critical in the preparation of nonnoble metal catalysts for the oxygen reduction reaction (ORR) in acidic medium. Nine commercial or developmental carbons have been used, as well as a synthetic carbon made by the pyrolysis of PTCDA in $NH_3/H_2/Ar$ atmosphere. This carbon is now labeled PTCDA T. Because our previous studies[32,37] demonstrated that nitrogen on the surface of the carbon supports was an essential requirement to obtain nonnoble metal-based catalytic sites, and that Fe-based catalysts displayed the highest performance for oxygen reduction in acidic media,[47] it was decided to use the carbon supports as received, but also to enrich their surfaces with nitrogen by treating them in $NH_3/H_2/Ar$ atmosphere before adsorbing iron-(II) acetate. The nominal Fe loading was set at 2000 ppm on the basis of results obtained with PTCDA, for which it was determined[46] that metallic particles usually surrounded by a carbon layer were detected at loadings higher than 0.5 wt % Fe. Therefore, this study details the properties of catalysts obtained by adsorption of iron(II) acetate on 19 [9 non-heat-treated (NT) and 10 heat-treated (T)] carbon supports.

It will be shown, on one hand, that the choice of carbon support has a large impact on the activity of these nonnoble metal catalysts and, on the other hand, that the expected benefit of increased area of the carbon support is not found under our experimental conditions.

Experimental Section

Synthesis of the Catalysts. The following carbon supports were investigated in this study: HS 300 (developmental graphite from Lonza), Printex XE-2 (Degussa Huls), Norit SX Ultra, Ketjenblack EC-600JD (Akzo Nobel), acetylene black (Chevron), Vulcan XC-72R (Cabot), Black Pearls 2000 (Cabot), a synthetic carbon made from PTCDA, and finally two developmental carbons from Sid Richardson carbons (RC1 and RC2). None of the commercial or developmental carbons were purified prior to catalyst synthesis; however, for the carbon made from PTCDA, the level of metallic impurities was lowered by HCl treatment. Details about purification procedures are given elsewhere.[46,47] The catalysts were generated on each of the carbons according to two synthetic procedures: Procedure 1 involves (i) adsorption of iron(II) acetate on carbon, followed by (ii) pyrolysis of the resulting powder at 900 °C in $NH_3/H_2/Ar$. Procedure 2 involves (i) pyrolysis of the carbon at 900°C in $NH_3/H_2/Ar$, (ii) adsorption of iron(II) acetate on the pyrolyzed carbon, followed by (iii) a second pyrolysis of the resulting powder at 900 °C in $NH_3/H_2/Ar$.

The different stages of the synthesis are now described in more detail. A calculated weight of iron(II) acetate (FeAc) was added to a suspension of carbon in deionized H_2O (dH_2O) to give a nominal concentration of 2000 ppm (0.2 wt %) of iron on carbon. For a few carbons, acetone was added to water to promote wetting and to facilitate their aqueous suspension. The effect of higher Fe loadings (0.5, 1, and 2 wt %) was also studied for a few carbons. The FeAc/carbon solution/suspension was stirred for 2 h. Then, water (and acetone) were completely evaporated, first with the help of a heating plate and finally in an oven at 75 °C overnight. About 0.5−1.0 g of the resulting dry powder was placed in a quartz boat and inserted into a 5-cm-diameter quartz tube. The tube was first purged with argon for 30 min. The pyrolysis stages of procedures 1 or 2 were performed as follows: A 2:2:1 mixture of $NH_3/H_2/Ar$ was continuously passed into the tube that was placed inside a split oven. The oven temperature was first raised to 400 °C, maintained at that level for 1 h, and then raised to 900 °C and maintained at that temperature for 1 h. The first temperature plateau was aimed at removing traces of water and/or organic impurities possibly adsorbed on the carbons. The catalysts at their different stages of synthesis are named carbon NT (not treated, as-received carbon), carbon NT + FeAc 2K (procedure 1 after stage ii, with 2K indicating that its nominal Fe loading was 2000 ppm), carbon T (procedure 2 after stage i), carbon T + FeAc 2K (procedure 2 after stage iii, with an Fe loading of 2000 ppm).

Physical and Chemical Characterizations of the Catalysts. The bulk concentration of iron in the synthesized catalysts was determined by neutron activation analysis (NAA) at the École Polytechnique de Montréal. Surface elemental analysis of the catalysts for all carbons was performed by X-ray photoelectron spectroscopy (XPS) using a VG Escalab 200i instrument. The Al K_α line (1486.6 eV) was chosen as the X-ray source. The

pass energy was 20 eV, and the energy increment was 100 meV. Narrow-scan photoelectron spectra were recorded (between four and eight scans) for N_{1s}, O_{1s}, and sometimes for the S_{2p} or Na_{1s} core levels only, but one scan was necessary for C_{1s}. The quantification of the detected elements and the deconvolution of the N_{1s} and O_{1s} spectra in their different peaks were performed using Casa software.

For specific surface area and pore size distribution measurements, about 0.150 g of each catalyst powder was investigated by N_2 gas-adsorption porosimetry (Micromeritics ASAP 2010). The adsorption isotherm was evaluated with the BJH model to give the pore size distribution of the powders.[50] The BET area was obtained fitting this model to the adsorption isotherm in the N_2 relative pressure range of 0.002−0.3.

Rotating Disk Electrode Experiments. The electrocatalytic activity for the oxygen reduction reaction (ORR) was studied with the rotating disk electrode (RDE) technique in O_2-saturated H_2SO_4 (pH = 1). The electrode preparation and measurement conditions have already been reported in detail.[32] The voltage between the electrode and a standard calomel electrode (SCE) was cycled at a sweep rate of 10 mV/s. A first cycle was performed with the electrode stationary and a second cycle with the electrode rotating at a rate of 1500 rpm. The RDE experiments were repeated for four electrodes for every catalyst, and the peak potential, V_{pr}, for the ORR represents the average of these four values.

From the RDE experiments, it was also possible to estimate the double-layer capacitance of each electrode in Ar-saturated H_2SO_4. The value of the capacitance per unit mass of catalyst, averaged within the swept potential window, was estimated from the following equation

$$C_{dl}\ (\text{in F/g}) = \int I_c\, dE/2\ v\Delta E m_{catalyst} \qquad (1)$$

where I_c stands for the capacitive current (in amperes) obtained during the cycle with the electrode being stationary, E is the electrode potential, v is the sweep rate in volts per second, ΔE is the scanned potential window (0.95 V), and $m_{catalyst}$ (in grams) is the mass of catalyst (Nafion excluded) deposited on the RDE. This latter was estimated to be 2×10^{-4} g according to the amount of ink applied.

Fuel Cell Experiments. Fabrication of the membrane electrode assembly (MEA) and testing of the catalysts in fuel cell was done as described below. The anode consisted of a 1-cm^2 ELAT electrode from E-TEK catalyzed with 0.37 mg cm^{-2} Pt (20 wt % Pt/C) that was further impregnated with a 5 wt % Nafion solution. The cathode support consisted of a 1-cm^2 uncatalyzed ELAT electrode. An ink was prepared from 12.9 mg of the catalyst powder dispersed in 500 μL of water and 300 μL of a 5 wt % Nafion solution, blended thereafter by ultrasonication for 1 h. Two (60 μL) aliquots of the ink were pipetted onto the hydrophilic side of the ELAT electrode. The electrodes were then placed in a vacuum oven at 75 °C for 1 h. The amount of dried catalyst (catalyst powder + Nafion) applied to the cathode varied between 3 and 4 mg of which about 40% was calculated to be Nafion. The MEA was prepared by hot pressing the electrodes onto a Nafion 117 membrane under 2500 psi (172 bar) at 140 °C for 40 s. All fuel cell measurements were performed at 80 °C. The O_2 and H_2 gas pressures were 60 and 30 psig (4.14 and 2.07 bar), respectively. The two gases were humidified at 105 °C prior to admission into the fuel cell. Before any measurements were performed, the fuel cell was left under open circuit conditions for 30 min. Then, a potential of 0.7 V vs RHE was applied during 2.5 h. Next, the resistance of the cell was measured by impedance, reading the real part of the impedance at high frequency where the imaginary part is 0. Finally, a polarization curve was recorded by varying the applied potential from 0.9 to 0.0 V vs RHE.

TABLE 1: Bulk Fe Content and Mass Loss for All Carbon Supports

	iron content (ppm)			mass loss during pyrolysis (% of initial mass)		
catalyst	NT[a]	NT + FeAc 2K[b]	T + FeAc 2K[c]	NT + FeAc 2K	T[d]	T + FeAc 2K
HS 300	NM[e]	2360	2520	13	9	14
Printex	NM	2280	2140	7	11	10
Norit	620	3180	2950	14	27	12
Ketjenblack	NM	1760	1810	10	19	11
acetylene black	NM	NM	1590	9	2	9
Vulcan	20	2020	1790	19	19	20
Black Pearls	NM	1950	1690	11	28	10
PTCDA	−	−	2190	−	69	27
RC1	70	2480	2310	20	35	16
RC2	NM	2650	2070	18	33	11

[a] NT = as-received. [b] NT + FeAc 2K = catalyst obtained by procedure 1 (see Experimental Section). [c] T + FeAc 2K = catalyst obtained by procedure 2 (see Experimental Section). [d] T = Carbon support obtained after the first pyrolysis in procedure 2. [e] NM = not measured.

Results

Actual Bulk Fe Content of the Catalysts. The actual bulk Fe contents for all NT + FeAc 2K and T + FeAc 2K catalysts (which include PTCDA T), as measured by NAA, are given in Table 1, where the estimated uncertainty is ca. ±5%. For most of the catalysts in Table 1, the Fe content was always >2000 ppm. Two possible factors might explain this high Fe concentration: (i) It is possible that the as-received carbon already contains some Fe impurities. A few of these as-received carbons were analyzed, and the results are reported in the NT column of Table 1. For instance, as-received Norit contains 620 ppm Fe that have to be added to the 2000 ppm nominal Fe adsorbed on all carbon supports. (ii) The second reason is that the aggressive character of NH_3 at high temperature leads to gasification of the carbon, increasing its surface area,[51−53] but also increasing the actual Fe content. The latter point is illustrated in Table 1, where we report the percentage loss during each pyrolysis relative to the mass prior to pyrolysis. Generally, the mass loss is much more important for carbon supports without FeAc (column T) than with FeAc (column NT+ FeAc). Because the heat treatment is the same for both materials, the only difference being the presence of 0.2 wt % Fe as iron acetate on the carbon support for NT + FeAc carbons, it can be concluded that the presence of FeAc decreases the aggressive behavior of NH_3 toward carbon under these experimental conditions. PTCDA T with 69% of initial mass loss is a special case because it is obtained by the pyrolysis of perylene tetracarboxylic dianhydride, which decomposes above 500 °C, releasing CO and CO_2 during polymerization of the perylene units. The mass losses reported in Table 1 are for samples heat-treated in a mixture of NH_3, H_2, and Ar, and not pure NH_3 as mentioned in refs 51−53. The individual effect of each gas was ascertained by heat-treating selected carbons (Vulcan and RC1) at 900 °C in Ar alone and in Ar + H_2. The percentage of initial mass loss during pyrolysis under these conditions were 0% (Vulcan) and 5% (RC1) for Ar alone and 2% (Vulcan) and 6% (RC1) for 1:1 Ar/H_2. It shows that the main mass losses reported in Table 1 result from the action of NH_3.

TABLE 2: XPS Results, Surface Concentrations of Elements

	surface concentration (at. %)											
	nitrogen				oxygen				sodium and sulfur			
catalyst[a]	NT[b]	NT + FeAc[b]	T[b]	T + FeAc[b]	NT	NT + FeAc	T	T + FeAc	NT	NT + FeAc	T	T + FeAc
HS 300	0.3	− −[c]	0.3	− −	5.7	0.4	0.3	0.6	− −	− −	− −	− −
Printex	− −	− −	− −	− −	0.3	0.4	− −	0.4	− −	− −	− −	− −
Norit	− −	1.1	1.9	1.3	2.7	1.1	0.8	0.9	0.2 Na	0.1 Na	0.1 Na	− −
Ketjenblack	− −	− −	0.8	0.6	0.5	0.5	0.4	0.3	− −	− −	− −	− −
acetylene black	− −	− −	− −	− −	0.3	0.1	0.1	0.2	− −	− −	− −	− −
Vulcan	− −	− −	1.1	0.7	0.6	0.3	0.5	0.3	0.3 S	0.1 S	− −	0.1 S
Black Pearls	− −	− −	0.6	0.9	1.1	0.7	0.5	0.7	0.2 S	− −	− −	− −
PTCDA	−	−	5.0	3.5	−	−	1.3	1.5	−	−	− −	− −
RC1	0.6	2.2	2.3	1.8	1.0	0.4	0.5	0.5	0.8 S	0.1 S	0.1 S	− −
RC2	− −	1.2	2.2	1.3	0.6	0.4	0.5	0.7	0.6 S	0.1 S	0.1 S	− −

[a] All catalysts prepared with 0.2 wt % Fe nominal loading. [b] For NT, NT + FeAc, T, and T + FeAc, see footnotes a−d of Table 1. [c] Cells with two dashes correspond to concentrations too low to be quantified.

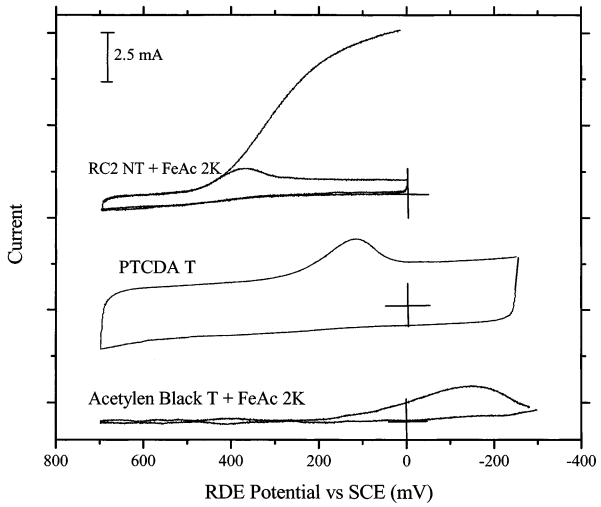

Figure 2. Cyclic voltammograms at 10 mV/s in O_2-saturated H_2SO_4 (pH = 1) of three catalysts showing various catalytic activities for the ORR. All RDE experiments were recorded at 0 and 1500 rpm, but only the 1500 rpm scan is shown for RC2 NT + FeAc 2K.

Surface N and O Contents of the Catalysts. The surface nitrogen and oxygen concentrations (in atom percent) were measured by XPS for all prepared catalysts and are reported in Table 2, along with N and O surface concentrations for the as-received carbon supports (column NT) and of the same carbon supports heat-treated in $NH_3/H_2/Ar$ (column T). The speciation of surface nitrogen and oxygen will be discussed later. Na and S were also detected by XPS in some of the carbons and the corresponding catalysts. Their surface concentrations are also reported in Table 2.

RDE and GDE Results. The cyclic voltammograms of three catalysts are presented in Figure 2. All three voltammograms display a peak for O_2 reduction. The potentials at the peak current, V_{pr}, for these three catalysts are quite different, spanning a potential range of about 600 mV. It indicates a large variation in the electrocatalytic activity between these three materials, the most catalytically active one being RC2 NT + FeAc 2K, because E for ORR under these conditions is 0.92 V vs SCE. The voltammogram of RC2 NT + FeAc 2K also shows a large current increase when the disk electrode rotates at 1500 rpm. The larger reduction current results from an increase of the oxygen concentration available at the electrode owing to the rotation.

The values of V_{pr} were used to compare the relative catalytic activity for ORR of all NT + FeAc and T + FeAc catalysts prepared for this study. The results are presented in Table 3. V_{pr} measurements for as-received carbons (NT) and carbons heat-treated (T) at 900 °C in 2:1:1 $NH_3/Ar/H_2$ are also given in Table 3 for comparison. Table 4 presents the V_{pr} values (and therefore the catalytic activity) for two carbon supports loaded at different Fe contents [between 0.2 wt % (2000 ppm) and 2 wt % Fe as iron acetate]. The following conclusions are drawn after examination of Tables 3 and 4: (i) Practically all catalysts containing Fe in Table 3 are more active than their respective carbon supports (NT or T). (ii) There is a large variation in the activity of all NT + FeAc and also all T + FeAc catalysts investigated. The nature of the support therefore plays a dominant role. (iii) Except for RC1 and RC2 in Table 3, there is always better catalytic activity going from NT + FeAc 2K to T + FeAc 2K catalyst using the same support. The difference in the preparation of both types of catalysts is the supplementary heat-treatment of the carbon support at 900 °C in 2:1:1 $NH_3/H_2/Ar$, which, as shown, improves the catalytic activity. (iv) The results of Table 4 indicate that the optimum Fe loading is between 0.2 and 1.0 wt % Fe as iron acetate and that there is no advantage in increasing the Fe content above 1 wt %. This

TABLE 3: Relative RDE ORR Catalytic Activity for Catalysts Containing 2000 ppm Fe

	peak potential (V_{pr}, mV vs SCE) for O_2 reduction peak at 0 rpm and 10 mV/s			
catalyst	NT[a]	NT+ FeAc 2K[a]	T[a]	T + FeAc 2K[a]
HS 300	−81	113	234	173
Printex	−93	−55	2	130
Norit	127	294	327	316
Ketjenblack	−144	71	204	255
acetylene black	<−350	−220	−186	−151
Vulcan	−220	168	37	301
Black Pearls	−130	153	285	268
PTCDA	−	−	108	315
RC1	−249	388	209	356
RC2	<−350	374	202	286

[a] For NT, NT + FeAc 2K, T, and T + FeAc 2K, see footnotes a−d of Table 1.

TABLE 4: Relative RDE ORR Catalytic Activity at Fe Contents Ranging from 0.2 to 2 wt %

	peak potential (V_{pr}, mV vs SCE) for O_2 reduction peak at 0 rpm and 10 mV/s			
catalyst	FeAc 0.2 wt %	FeAc 0.5 wt %	FeAc 1 wt %	FeAc 2 wt %
Vulcan T + FeAc	301	360	323	285
RC1 NT + FeAc	388	371	278	103
RC1 T + FeAc	356	434	443	404

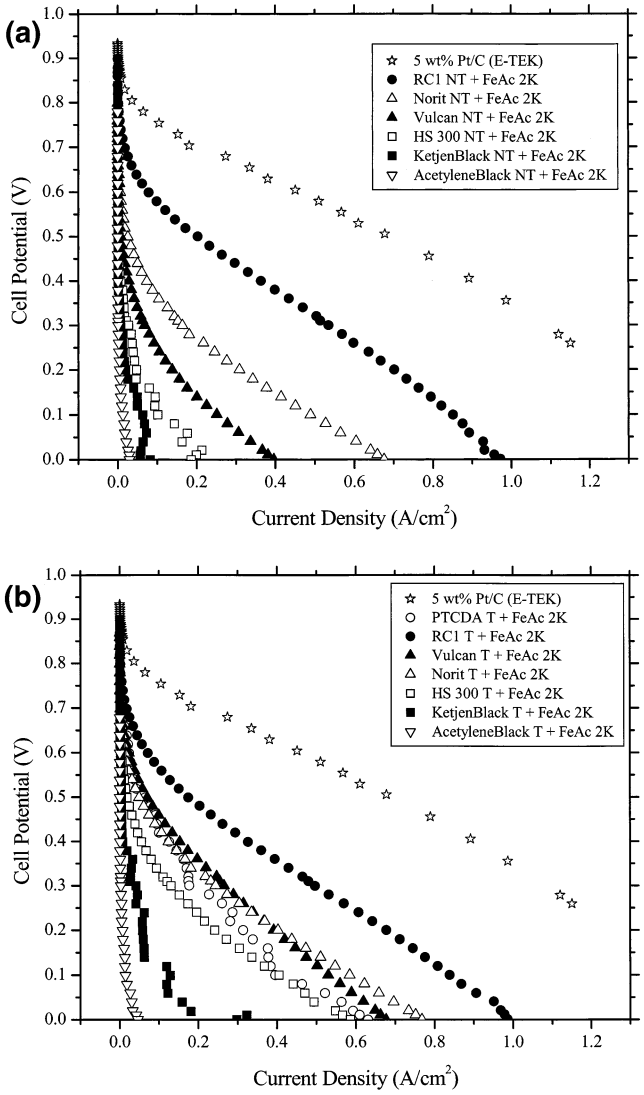

Figure 3. GDE polarization curves recorded at 80 °C for a single membrane electrode assembly using selected carbons: (a) NT + FeAc 2K, (b) T + FeAc 2K.

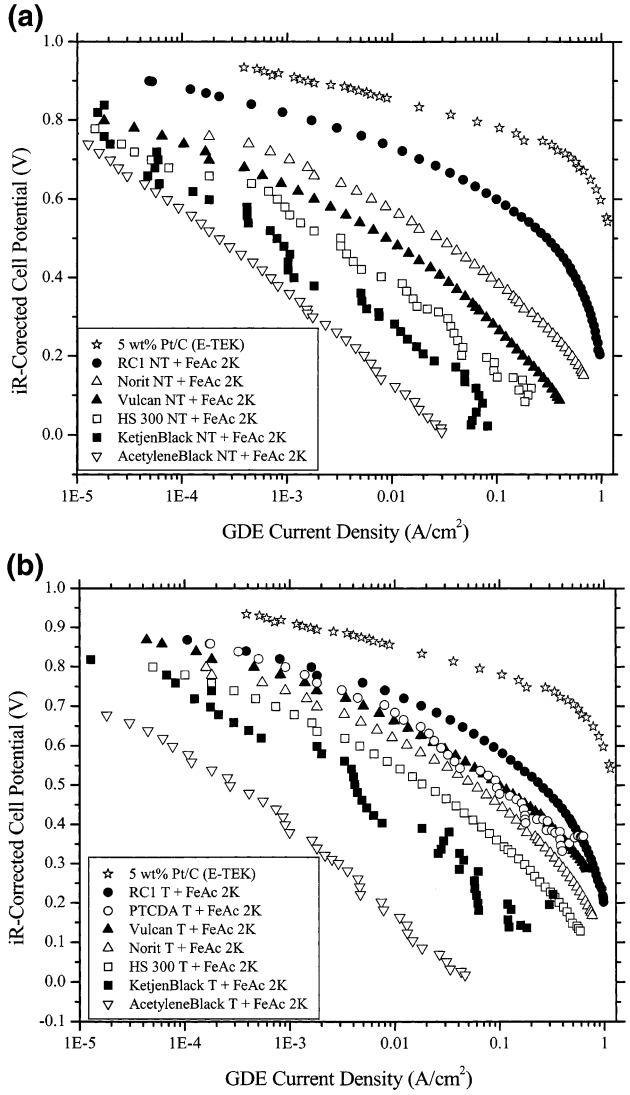

Figure 4. Tafel plots for the GDE polarization curves for selected carbons: (a) NT + FeAc 2K, (b) T + FeAc 2K.

conclusion is similar to that of PTCDA-based catalysts for which it was shown that Fe metal or carbide particles surrounded by carbon appeared for Fe loadings higher than 0.5 wt %.[46] It must be noted, however, that the optimal Fe loading is strongly influenced by the carbon support as well as the preparation procedure.

Gas diffusion electrode (GDE) polarization curves are presented in Figure 3a for selected NT + FeAc 2K carbons and in Figure 3b for the same carbons pretreated as T + FeAc 2K. A polarization curve obtained under the same conditions with 5 wt % Pt/C (E-TEK) is given for comparison. The following conclusions can be drawn from Figure 3a and b:

(i) There is a large difference in the fuel cell performance of all NT + FeAc and T + FeAc catalysts. The changes in performance observed in the GDE experiments vary in accordance with the changes in the catalytic activity observed in RDE experiments.

(ii) Except for RC1, there is an improvement in GDE performance going from NT + FeAc 2K type catalysts for each carbon support to T + FeAc 2K type catalysts for the same carbon support. It is with Vulcan that the improvement in performance is the most significant. Once heat-treated according to procedure 2, Vulcan T + FeAc 2K becomes equivalent to PTCDA T + FeAc 2K and Norit T + FeAc 2K. RC1 NT + FeAc 2K and RC1 T + FeAc 2K display an equivalent performance, which is well above the performance displayed by the other carbon supports.

Figure 4a and b presents the Tafel plots for the GDE polarization curves of Figure 3a and b. The cell potentials have been *iR* corrected. Tafel slopes for ORR are obtained from the linear region at low current density (the polarization at the anode is assumed to be negligible). For NT + FeAc 2K prepared samples, the Tafel slopes vary from −73 mV/decade for RC1 to −183 mV/decade for acetylene black, whereas for the T + FeAc 2K prepared samples, the variation is from −74 mV/decade for RC1 to −168 mV/decade for acetylene black. The Tafel slope for 5 wt % Pt/C is −67 mV/decade.

Porosimetry Investigation and Double-Layer Capacitance. The pore structure of each catalyst labeled as NT + FeAc 2K or T + FeAc 2K was evaluated. Table 5 shows the total BET area of all NT + FeAc 2K catalysts, as well as the absolute value of the surface area provided by three pore intervals (macropores, 300−10 nm; mesopores, 10−1.7 nm; and micropores, <1.7 nm) for the same catalysts. The areas corresponding to the macro- and mesopores were estimated from the adsorption isotherm and the BJH model. The area provided by pores having a dimension less than 1.7 nm was calculated

TABLE 5: BET Areas and Surface Area Distributions

catalyst[a]	total BET surface area ($m^2\ g^{-1}$)	surface area ($m^2\ g^{-1}$) macropores 300−10 nm	mesopores 10−1.7 nm	micropores <1.7 nm
HS 300 NT + FeAc	265	40	185	40
HS 300 T + FeAc	+0	+0	+0	+0
Printex NT + FeAc	965	145	710	110
Printex T + FeAc	+5	+20	+10	−25
Norit NT + FeAc	1230	50	460	720
Norit T + FeAc	+230	+15	+45	+170
Ketjenblack NT + FeAc	1310	200	1055	55
Ketjenblack T + FeAc	+55	+55	+80	−55
acetylene black NT + FeAc	75	20	60	0
acetylene black T + FeAc	+20	+0	+15	+0
Vulcan NT + FeAc	250	35	115	100
Vulcan T + FeAc	+150	+5	+145	+0
Black Pearls NT + FeAc	1450	185	545	720
Black Pearls T + FeAc	+60	+25	+430	−395
PTCDA T + FeAc	370	25	145	200
RC1 NT + FeAc	335	70	70	195
RC1 T + FeAc	+345	+20	+260	+65
RC2 NT + FeAc	475	100	105	270
RC2 T + FeAc	+205	+20	+220	−35

[a] All catalysts prepared with 0.2 wt % Fe nominal loading. [b] For NT + FeAc and T + FeAc, see footnotes b and c of Table 1.

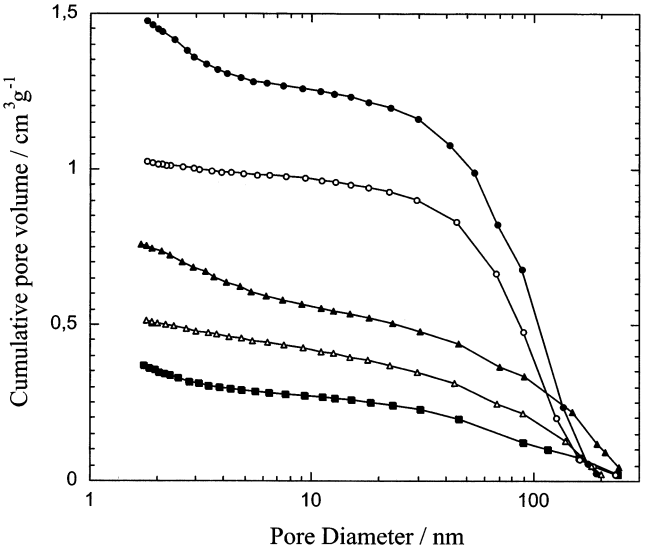

Figure 5. Typical pore size distribution for meso and macropores for catalysts prepared on three carbon supports: PTCDA T (squares), Vulcan (triangles), and RC1 (circles). Open and solid symbols correspond to catalysts prepared as NT + FeAc 2K and T + FeAc 2K, respectively.

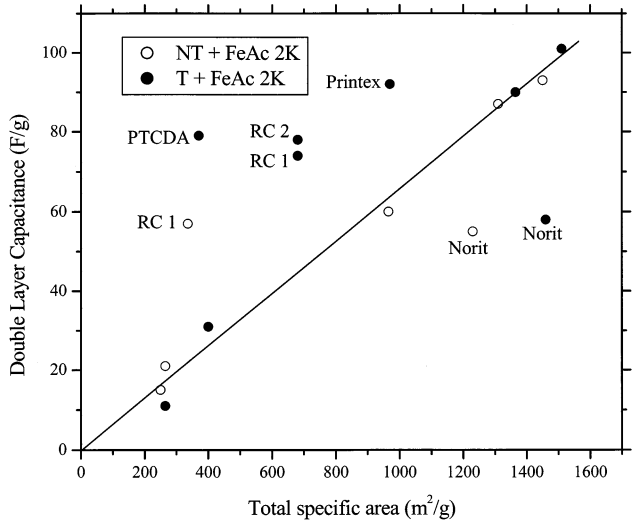

Figure 6. Double-layer capacitance of each catalyst vs total specific surface area of the same catalysts.

as the difference between the total BET area and the sum of the areas provided by macro- and mesopores. For all T + FeAc 2K catalysts, Table 5 presents the change in surface area compared to that of the corresponding NT + FeAc 2K catalysts. Thus, a plus sign represents an increase in surface area from procedure 1 to procedure 2, whereas a minus sign indicates a decrease in surface area. The studied carbons have BET areas ranging from 75 to 1510 $m^2\ g^{-1}$. The distribution of the pore sizes differs markedly among these catalysts. The surface area imparted to the macropores is never dominant but can represent up to 25% of the BET area. The major part of the surface area is provided by either meso- or micropores. A typical example of the pore size distribution for meso- and macropores is illustrated in Figure 5 for three types of carbon supports. This figure depicts the cumulative pore volume in cubic centimeters per gram of catalyst powder, with the cumulative volume of 0 cm^3/g referring to the highest pore diameter measured with this technique.

Let us now consider the effect of the additional pyrolysis of procedure 2 on the pore structure of the catalytic powders. For a given carbon type, the total BET area of the catalysts prepared as T + FeAc 2K is always larger than those prepared as NT + FeAc 2K. This is also true for the surface areas of the mesopores and of the macropores, which increase for all catalysts. As for the micropores, the surface areas either increase (Norit, RC1) or decrease by conversion of the micropores to larger pores (Printex, Ketjenblack, Black Pearls, RC2). PTCDA is a particular case because FeAc is adsorbed only on the carbon support PTCDA T + FeAc.

Figure 6 presents the variation of the double-layer capacitance of each catalyst (in farads per gram of catalyst) as a function of the total specific surface area (in square meters per gram of catalyst). The slope of the straight line in Figure 6 is 0.07 F/m^2, which is the capacitance related to a unit surface area of these catalysts. Values of 0.1 and 0.08 F/m^2 were found for Norit SX Plus in 1 M H_2SO_4 and for Vulcan XC-72 in 2 M H_2SO_4, respectively.[54] At first sight, when comparing capacitances in Figure 6 and catalyst ORR activities in Table 3 (and/or Figure 3a and b), it might appear that high catalytic activities correlate

with increasing capacitance, as is found for PTCDA, RC1, and RC2. These catalysts lie above the straight line in Figure 6 and hence have a capacitance larger than 0.07 F/m^2. However, Printex T + FeAc 2K also lies above the 0.07 F/m^2 line, and yet, it has a low ORR activity. Also, both Norit NT and T + FeAc 2K lie below 0.07 F/m^2 but give a high catalytic activity. The conclusion here is that the catalytic activity is not influenced by the capacitance per unit surface area of the catalyst support.

Discussion

Relation between the RDE Peak Potential, V_{pr}, and the GDE Polarization Curves. To initiate this discussion, let us first start from Figure 4a and b, which displays the semilogarithmic (or Tafel) polarization curves. The experimental Tafel slope for Pt in both plots is −67 mV/decade.

The reduction of oxygen on Pt has been extensively studied in acidic medium. Equation 2 represents the first electron transfer of the ORR. This reaction is known to be the rate-determining step.[55,56]

$$O_2 + H_3O^+ + e^- \rightarrow O_2H_{ads} + H_2O \qquad (2)$$

At low current densities, it has been shown that the ORR occurs on a highly oxide-covered Pt surface (Temkin condition) with a Tafel slope ($-2.303RT/\alpha_r F$) of −60 mV/decade at room temperature. Here, R, T, α_r, and F are the molar gas constant, the absolute temperature, the transfer coefficient, and the Faraday constant, respectively. A value of −60 mV means that $\alpha_r = 1$.[57−59] Under these conditions, the theoretical value of the Tafel slope at 80 °C (the temperature at which the polarization curves were recorded) is −70 mV/decade, in good agreement with the slope of −67 mV/decade found experimentally.

Because the Tafel slopes on the best nonnoble catalysts at low current densities are similar to the Tafel slope on Pt, one can conclude that the ORR kinetics on these catalysts are similar to the ORR kinetics on Pt. However, the nonnoble catalysts of lower activity display larger Tafel slopes (up to −183 mV/decade for acetylene black NT + FeAc 2K in Figure 4a and up to −168 mV/decade for the T + FeAc prepared catalysts supported on the same carbons in Figure 4b). This larger Tafel slope for the poor catalysts might stem from a different reaction mechanism for ORR, and we correlate it to the existence of a different catalytic site between the poor and the other catalysts, as will be discussed later. For the other catalysts (i.e., those not supported on acetylene black, Printex, or Ketjenblack in Figures 3 and 4), the kinetics for oxygen reduction proceeds in a manner similar to that on Pt, and they yield Tafel slopes in the range of −70 to −95 mV/decade. The difference in electrocatalytic activity among these materials is therefore most probably due to a change in the total number of active sites created on the particular carbon support. Assuming that α_r is constant for these catalysts, it is now possible to discuss the meaning of V_{pr} as an important parameter in the comparison of various catalysts.

In the RDE measurements, when the electrode potential is scanned in the cathodic direction in the region of the ORR onset, the current increases through kinetic activation up to a point where this effect is exactly counterbalanced by a decreased concentration of oxygen at the electrode surface araising because of mass-transport limitations. The result of this interplay is that the current reaches a maximum value, which defines the peak potential V_{pr} (see Figure 2). V_{pr} is thus the result of kinetic as well as oxygen-transport properties. One can apply the result obtained for planar electrodes. For an irreversible reduction reaction that is first-order in reactant concentration, the following equation can be found[60]

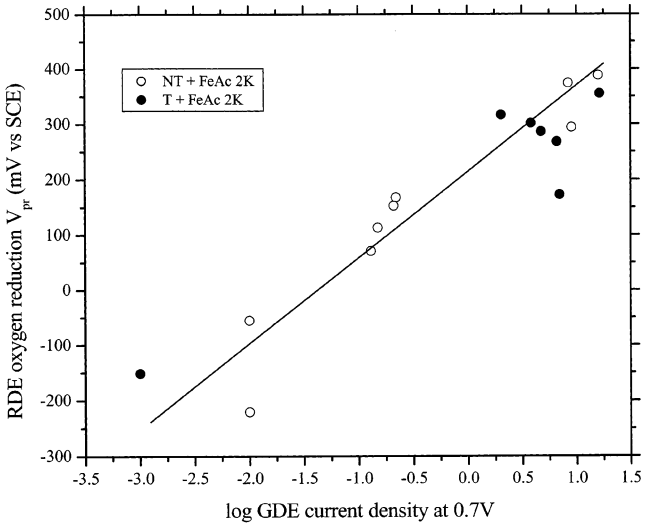

Figure 7. Linear relationship between V_{pr} from RDE and the logarithm of the current density at 0.7 V from GDE.

$$V_{pr} = E^\circ + (RT/\alpha_r F)[\ln(k^\circ/D^{1/2}) - 0.5\ln(\alpha_r F\upsilon/RT) - 0.78] \qquad (3)$$

where E°, in our case, is the standard potential for the ORR; D is the oxygen diffusion coefficient in the electrolyte; k° is the reaction rate at standard potential for ORR of the electrode; and υ is the sweep rate. From eq 3, it is evident that a 10-fold increase in k° raises V_{pr} by a value equal to the Tafel slope, $RT\ln[10/(\alpha_r F)]$, if the other parameters (especially α_r) are kept constant. Thus, assuming a constant value for α_r, the variation in peak potential between two different catalysts is related to the change in k° as follows

$$\Delta V_{pr} = (RT/\alpha_r)\Delta\ln(k^\circ), \qquad \text{valid for constant } \alpha_r \qquad (4)$$

k° is directly related to the density of the catalytic sites on the carbon support if one assumes that the catalytic sites display identical activity, regardless of the support.

It is now shown how the values of V_{pr} obtained from RDE experiments can be related to the polarization curves of GDE with the help of eq 3. This equation shows that $\ln(k^\circ)$ is related to V_{pr} by a linear relation. On the other hand, the Tafel relation stipulates that the current density obtained for a given potential (0.7 V vs RHE) is proportional to k°. Thus, the logarithm of the current obtained at a given potential in the polarization curve should have a linear relation with V_{pr}. This is indeed what is shown in Figure 7. For the Tafel relation to be valid, the chosen potential must be such that the GDE current is measured in the Tafel region of the polarization curve. From this part of the discussion, it can therefore be concluded that V_{pr} is a valid parameter for expressing and comparing the catalytic activity.

Relation between the RDE Peak Potential and the Nitrogen Surface Concentration. Figure 8 presents the relation between the activity of the catalysts (expressed as RDE ORR peak, V_{pr}) and the total nitrogen surface content in atom percent. This relation is composed of two linear parts. It has already been demonstrated[37] that nitrogen is an essential element in obtaining OR activity from nonnoble metals. Furthermore, it is an integral component of the two catalytic site types (FeN_2/C and FeN_4/C) detected at the surface of the catalysts supported on PTCDA T.[49] The observed increase in catalytic activity with increasing total N content shown in Figure 8 is therefore

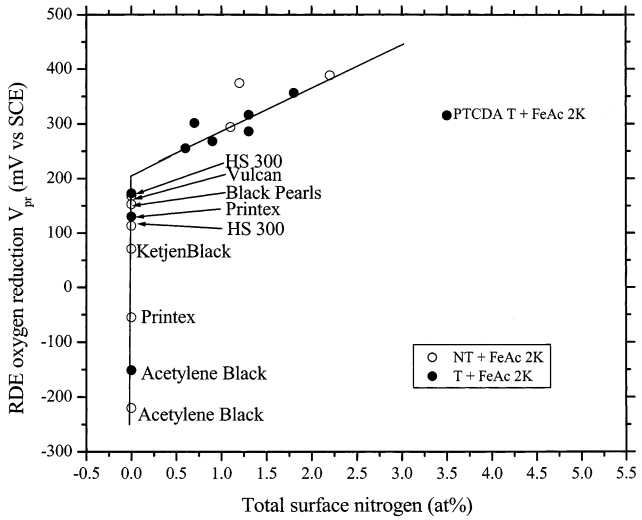

Figure 8. Change in catalytic activity (from V_{pr}) with total N surface concentration of the catalysts from XPS results.

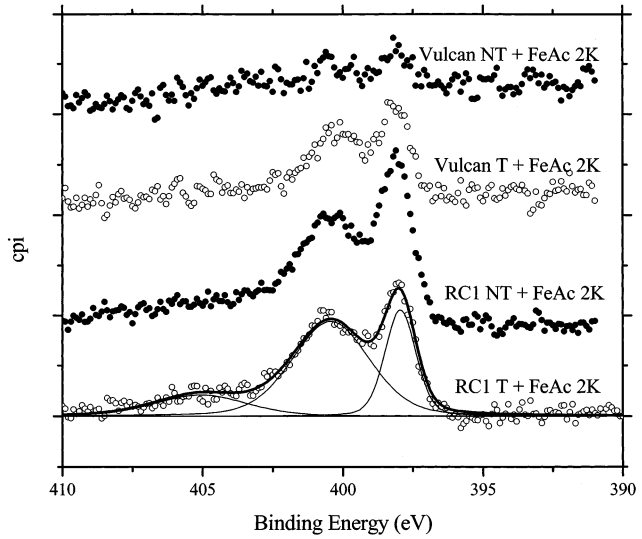

Figure 9. XPS narrow-scan spectra for N_{1s} for four catalysts. The spectrum for RC1 T + FeAc 2K has been deconvoluted.

expected. Only the PTCDA T + FeAc 2K catalyst is not on the straight line, being less active than expected.

It was also previously demonstrated that the catalytic sites were made of pyridinic-type nitrogens.[46] Figure 9 presents the N_{1s} narrow-scan spectrum of four catalysts studied here along with the fitted deconvolution of the spectrum of RC1 T + FeAc 2K using three peaks:[61−63] pyridinic (398.0 eV), pyrrolic (401.0 eV) and graphitic (403.9 eV). The narrow-scan spectra for all other catalysts are similar to those in Figure 9, but the fitting

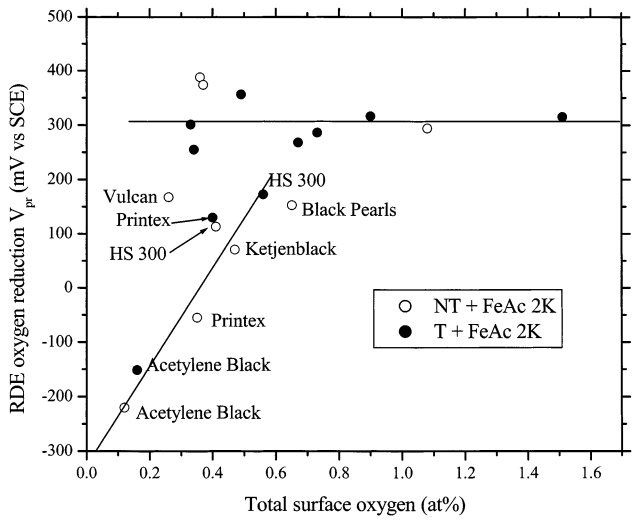

Figure 10. Change in catalytic activity (from V_{pr}) with total O surface concentration of the catalysts from XPS results.

was performed only for the catalysts displaying an acceptable signal-to-noise ratio. The deconvolution fit results are presented in Table 6. From this table, one notices that the percentage of pyridinic-type nitrogen for all the catalysts is always 36 ± 10%. If we suppose, as we have reported elsewhere,[46] that this pyridinic type of nitrogen is the important nitrogen component of the most active catalytic sites, then the fact that the proportion of the pyridinic nitrogen (relative to the total nitrogen content) is quite constant for all catalysts explains why the variation in the total nitrogen content accounts for the ORR activity of the catalysts in Figure 8.

A second part in Figure 8 shows a rather unexpected result. The vertical line demonstrates that there is some catalytic effect even for the samples that contain very little or no nitrogen. The carbon supports are identified for that vertical part of the graph and will be discussed further below when we examine oxygen concentration in Figure 10.

Relation between the RDE Peak Potential and the Oxygen Surface Concentration. Figure 10 presents the relation between the catalytic activity and the total surface concentration of oxygen, and as was the case in Figure 8, it is composed of two linear regions. In the first region, a linear correlation between the ORR activity and the surface oxygen content is observed, characterizing the catalysts with low activity. The names of the carbon supports written in full in Figure 10 are the same than those in Figure 8. One can therefore conclude that, when there is no nitrogen at the surface of the support (vertical line in Figure 8) to produce the N-containing catalytic sites (FeN_2/C and/or FeN_4/C), a third type of catalytic site is responsible for the remaining low ORR activity. On the basis of Figure 10, it is

TABLE 6: XPS Results, Fitted Deconvolutions of N_{1s} Spectra

	% of total N atoms											
	pyridinic				pyrrolic				graphitic			
catalyst[a]	NT[b]	NT + FeAc[b]	T[b]	T + FeAc[b]	NT	NT + FeAc	T	T + FeAc	NT	NT + FeAc	T	T + FeAc
Norit	− −[c]	38	23	47	− −	55	46	23	− −	7	31	30
Ketjenblack	− −	− −	32	− −	− −	− −	47	− −	− −	− −	21	− −
Vulcan	− −	− −	27	32	− −	− −	32	68	− −	− −	41	0
Black Pearls	− −	− −	40	44	− −	− −	33	25	− −	− −	26	31
PTCDA	−	−	33	37	−	−	37	34	−	−	25	27
RC1	34	33	34	26	49	41	44	58	17	26	23	16
RC2	− −	33	30	33	− −	35	34	47	− −	32	36	20

[a] All catalysts prepared with 0.2 wt % Fe nominal loading. [b] For NT, NT + FeAc, T, and T + FeAc, see footnote of Table 1. [c] Cells with two dashes correspond to N_{1s} spectra with signal-to-noise ratios too poor to be deconvoluted.

TABLE 7: XPS Results, Fitted Deconvolutions of O_{1s} Spectra

	% of total O atoms											
	O_A (533.3 ± 0.02 eV)				O_B (531.8 ± 0.03 eV)				O_C (530.4± 0.04 eV)			
catalyst[a]	NT[b]	NT[b] + FeAc	T[b]	T[b] + FeAc	NT	NT + FeAc	T	T + FeAc	NT	NT + FeAc	T	T + FeAc
HS300	60	44	52	34	40	47	48	47		9	–	19
Printex	43	55	–	50	57	45	–	45		–	–	5
Norit	52	– –[c]	29	17	48	– –	61	52		– –	10	31
Ketjenblack	52	53	55	47	48	38	45	53	–	9	–	–
acetylene black	52	50	38	50	48	50	62	50	–	–	–	–
Vulcan	49	50	50	40	51	43	50	54		7		6
Black Pearls	48	34	44	40	52	48	56	60	–	18	–	–
PTCDA	–	–	38	32	–	–	51	45	–	–	11	23
RC1	58	28	39	36	42	42	48	46		30	13	18
RC2	51	36	44	35	37	45	51	41	12	19	4	24

[a] All catalysts prepared with 0.2 wt % Fe nominal loading. [b] For NT, NT + FeAc, T, and T + FeAc, see footnotes a−d of Table 1. [c] Cells with two dashes correspond to O_{1s} spectra with signal-to-noise ratios too poor to be deconvoluted.

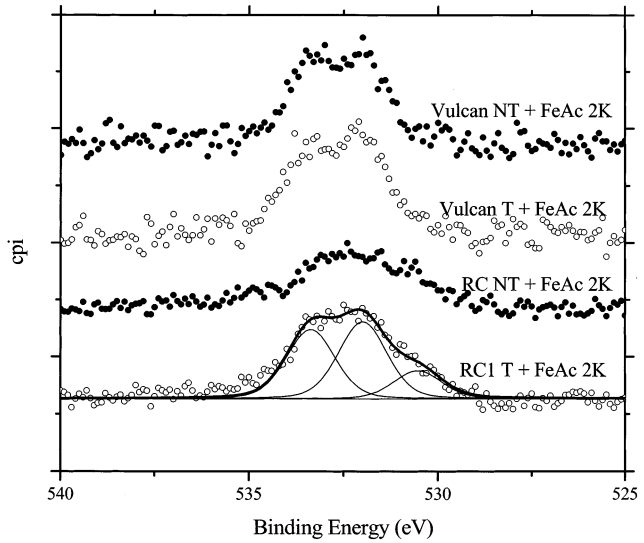

Figure 11. XPS narrow-scan spectra for O_{1s} for four catalysts. The spectrum of RC1 T + FeAc 2K has been deconvoluted.

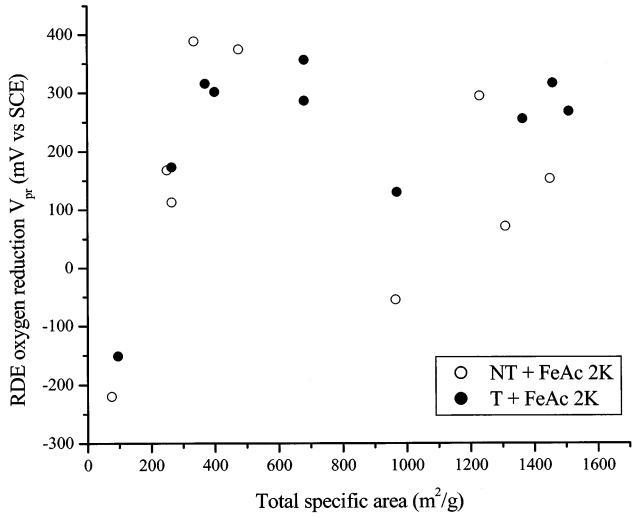

Figure 12. Change in catalytic activity (from V_{pr}) with total specific surface area of the catalysts from gas-adsorption BET.

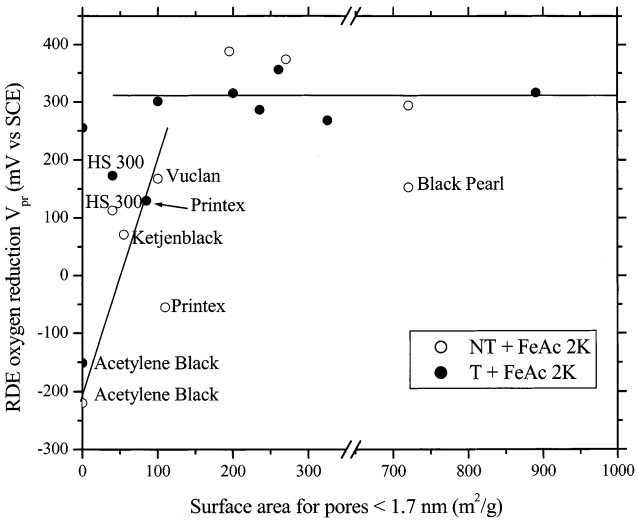

Figure 13. Change in catalytic activity (from V_{pr}) with micropore surface area of the catalysts from gas-adsorption BET.

proposed that this third site is an iron oxide, because the low ORR activity correlates linearly with the surface oxygen content and it has also been demonstrated[37,46] that there is no ORR activity without metal (Fe, in the present study). The second region of Figure 10 concerns the supports that contain surface nitrogen. In this case, the catalysts are much more active, and their catalytic activity is independent of the surface oxygen concentration, provided that this oxygen concentration is at least ∼0.4 at. %.

The XPS O_{1s} narrow-scan spectrum of oxygen is presented for four catalysts in Figure 11. The spectrum for RC1 T + FeAc 2K is deconvoluted into three components: O_A (533.3 eV), O_B (531.8 eV), and O_C (530.4 eV). Similar spectra are also obtained for the other catalysts, but sometimes the deconvolution involves only O_A and O_B. All fitted deconvolution results are given in Table 7. O_A with a binding energy of ∼533.3 eV is assigned to the C−OH and/or C−O−C groups, whereas O_B with a binding energy of ∼531.8 is assigned to C═O (aldehydes, ketones, lactones) or S═O (sulfone, sulfates).[64−66] O_C with a binding energy of 530.4 eV is characteristic of metal-bound oxygen.[67−69] The presence of O_C in the O_{1s} spectrum of RC1 T + FeAc 2K in Figure 11 indicates that the catalytic iron oxide site is also present in this catalyst even if this particular site does not contribute very much to the total catalytic activity.

Relation between the RDE Peak Potential and the Surface Area of the Carbon Support. One of the parameters that differentiates the carbon supports is their specific surface areas. Intuitively, one would expect that a larger specific surface area would lead to a greater extent of precursor adsorption giving a higher concentration of the catalytic sites, resulting therefore in better catalytic activity. Figure 12 shows that there is no relation between the catalytic activity and the total specific

surface area of the supports as measured from gas-adsorption BET. It is noted in Figure 12 that there are indeed very active catalysts, e.g., RC1 NT + FeAc 2K, that are characterized by moderate specific surface areas (see Table 5) and rather inactive catalysts characterized by larger specific surface areas. If the specific surface area is deconvoluted into the different ranges of pore size, there is again no correlation between the catalytic activity and the surface area of the macropores or the mesopores of the supports. There does seem, however, to be a weak correlation between the catalytic activity and the surface areas of the micropores as shown in Figure 13. This relationship is similar to the one already shown in Figure 10 for the oxygen contents of the supports devoid of surface nitrogen. In fact, the same carbon supports are encountered in the linear part of the curve (except for Black Pearls). This would mean that the catalytic iron oxide would be associated with the presence of the micropores in the support. There is no influence of the micropores anymore for the more performing catalysts for which a significant amount of N is found at the surface.

Conclusions

In this work, various catalysts for the electroreduction of O_2 in acidic medium were prepared by pyrolyzing at 900 °C in an NH_3-containing atmosphere iron acetate adsorbed on 19 different carbon supports. The goal of this work was to establish whether the carbon support was an important factor in determining the catalytic activity. All the catalysts were analyzed for specific surface area, porosity distribution, and N and O surface contents, as well as for their respective electrochemical activities for O_2 reduction.

It is obvious that the catalytic activity varies greatly from one support to another, but the specific surface area of the catalysts is not an essential factor in obtaining high activity for ORR. The most important factor is surface N content. This can be explained by considering the fact that N is known to be part of the two major catalytic sites (FeN_4/C and FeN_2/C) for catalytic materials obtained by using iron(II) acetate and NH_3 as Fe and N precursors.

It has been demonstrated that it is possible to enrich the various carbon supports in N before adsorbing iron(II) acetate. This N enrichment improves the catalytic activity of the materials supported on the carbons that we have examined, the most dramatic example being that of Vulcan XC-72R, which, after treatment, joins the group of good carbon supports that includes PTCDA T, Norit T, Blackpearl T, and Ketjenblack T. The best carbon supports are incontestably as-received RC1 and RC2, whereas the worst ones are acetylene black, Printex, and HS300, which are impossible to enrich in nitrogen under the conditions used in this study.

It is also clear from this study that supports completely devoid of N display some catalytic activity that varies with the amount of surface oxygen. This oxygen content, added to the fact that an XPS O_{1s} peak assigned to oxygen bound to metal is detected, suggests that the catalytic site for O_2 reduction in these materials is an iron oxide. This catalytic site also occurs in all other catalysts where an XPS O_{1s} peak of Fe bound to oxygen is also detected (see, for instance, the O_{1s} XPS spectrum of RC1 NT + FeAc 2K in Figure 11 and Table 7). Therefore, there are three catalytic sites at work in these catalysts: an iron oxide and the FeN_4/C and FeN_2/C catalytic sites, with the latter being responsible for most of the measured activity for oxygen reduction. The iron oxide catalytic site has to be in a form that protects it from dissolution in the acidic medium (pH = 1) used for the experiments. There seems to be a relation between the specific surface area of the micropores in these catalysts and the concentration of the iron oxide catalytic sites. It is necessary to study this relation in more detail to understand its actual meaning.

Acknowledgment. The authors thank all producers that donated carbon samples. This work was supported by the National Sciences and Engineering Council of Canada (NSERC), and the Swedish Foundation for Strategic Environmental Research (MISTRA). One of the authors (F.J.) is grateful to The Royal Swedish Academy of Sciences for a Hans Werthén grant. J.P.D. thanks Marck Lefebvre from MPI Inc. for his several suggestions and comments about this work.

References and Notes

(1) Gottesfeld, S.; Zawodzinski, T. A. *Adv. Electrochem. Sci. Eng*. **1997**, *5*, 195.
(2) Ralph, T. R.; Hogarth, M. P. *Platinum Met. Rev*. **2002**, *46*, 3.
(3) Wiesener, K. *Electrochim. Acta* **1986**, *31*, 1073.
(4) Wiesener, K.; Ohms, D.; Neumann, V.; Franke, R. *Mater. Chem. Phys.* **1989**, *22*, 457.
(5) Tarasevich, M. R.; Zhutaeva, G. V.; Radyushkina, K. A. *Russ. J. Electrochem.* **1995**, *31*, 1064 (Translation of *Electrokhimiya*).
(6) Tarasevich, M. R.; Radyuskina, K. A. *Mater. Chem. Phys.* **1989**, *22*, 477.
(7) Scherson, D.; Tanaka, A. A.; Gupta, S. L.; Tryk, D.; Fierro, C.; Holze, R.; Yeager, E. B.; Latimer, R. P. *Electrochim. Acta* **1986**, *31*, 1247.
(8) Tanaka, A.; Gupta, S. L.; Tryk, D.; Fierro, C.; Yeager E. B.; Scherson, D. A. In *Structural Effects in Electrocatalysis and Oxygen Electrochemistry*; Scherson, D., Tryk, D., Daroux, M., Xing, X., Eds.; The Electrochemical Society, Inc.: Pennington, NJ, 1992; Vol. 92-11, p 555.
(9) Gojkovic, S. L.; Gupta, S.; Savinell, R. F. *J. Electrochem. Soc.* **1998**, *145*, 3493.
(10) Gojkovic, S. L.; Gupta, S.; Savinell, R. F. *J. Electroanal. Chem.* **1999**, *462*, 63.
(11) Gojkovic, S. L.; Gupta, S.; Savinell, R. F. *Electrochim. Acta* **1999**, *45*, 889.
(12) van Veen, J. A. R.; Colijn, H. A.; van Baar, J. F. *Electrochim. Acta* **1988**, *33*, 801.
(13) Sun, G. Q.; Wang, J. T.; Gupta, S.; Savinell, R. F. *J. Appl. Electrochem.* **2001**, *31*, 1025.
(14) Bouwkamp-Wijnoltz, A. L.; Visscher, W.; van Veen, J. A. R. *Electrochim. Acta* **1998**, *43*, 3141.
(15) Biloul, A.; Gouérec, P.; Savy, M.; Scarbeck, G.; Besse, S.; Riga, J. *J. Appl. Electrochem.* **1996**, *26*, 1139.
(16) Gouérec, P.; Biloul, A.; Contamin, O.; Scharbeck, G.; Savy, M.; Riga, J.; Weng, L. T.; Bertrand, P. *J. Electroanal. Chem.* **1997**, *422*, 61.
(17) Gouérec, P.; Savy, M.; Riga, J. *Electrochim. Acta* **1998**, *43*, 743.
(18) Gouérec, P.; Savy, M. *Electrochim. Acta* **1999**, *44*, 2653.
(19) Contamin, O.; Debiemme-Chouvy, C.; Savy, M.; Scarbeck, G. *Electrochim. Acta* **1999**, *45*, 721.
(20) Contamin, O.; Debiemme-Chouvy, C.; Savy, M.; Scarbeck, G. *J. New Mater. Electrochem. Syst.* **2000**, *3*, 67.
(21) Ladouceur, M.; Lalande, G.; Guay, D.; Dodelet, J. P.; Dignard-Bailey, L.; Trudeau, M. L.; Schulz, R. *J. Electrochem. Soc.* **1993**, *140*, 1974.
(22) Lalande, G.; Côté, R.; Tamizhmani, G.; Guay, D.; Dodelet, J. P.; Dignard-Bailey, L.; Weng, L. T.; Bertrand, P. *Electrochim. Acta* **1995**, *40*, 2635.
(23) Faubert, G.; Côté, R.; Guay, D.; Dodelet, J. P.; Dénes, G.; Bertrand, P. *Electrochim. Acta* **1998**, *43*, 341.
(24) Sawaguchi, T.; Itabashi, T.; Matsue T.; Uchida, I. *J. Electroanal. Chem.* **1990**, *279*, 219.
(25) Widelöv, A. *Electrochim. Acta* **1993**, *38*, 2493.
(26) Claude, E.; Addou, T.; Latour, J. M.; Aldebert, P. *J. Appl. Electrochem.* **1998**, *28*, 57.
(27) Okada, T.; Gokita, M.; Yuasa, M.; Sekine, I. *J. Electrochem. Soc.* **1998**, *145*, 815.
(28) Okada, T.; Gotou, S.; Yoshida, M.; Yuasa, M.; Hirose, T.; Sekine, I. *J. Inorg. Organomet. Polym.* **1999**, *9*, 199.
(29) Okada, T.; Yoshida, M.; Hirose, T.; Kasuga, K.; Yu, T.; Yuasa, M.; Sekine, I. *Electrochim. Acta* **2000**, *45*, 4419.
(30) Jiang, R.; Chu, D. *J. Electrochem. Soc.* **2000**, *147*, 4605.
(31) van Wingerden, B.; van Veen, J. A. R.; Mensch, C. T. J. *J. Chem. Soc., Faraday Trans. 1* **1988**, *84*, 65.
(32) Lefèvre, M.; Dodelet, J. P., Bertrand, P. *J. Phys. Chem. B* **2000**, *104*, 11238.

(33) Bae, I. T.; Tryk, D. A.; Scherson, D. A. *J. Phys. Chem. B* **1998**, *102*, 4114.
(34) Gupta, S.; Tryk, D.; Bae, I.; Aldred, W.; Yeager, E. *J. Appl. Electrochem.* **1989**, *19*, 19.
(35) Ohms, D.; Herzog, S.; Franke, R.; Neumann, V.; Wiesener, K.; Gamburcev, S.; Kaisheva, A.; Iliev, I. *J. Power Sources* **1992**, *38*, 327.
(36) Martin Alves, M. C.; Tourillon, G. *J. Phys. Chem.* **1996**, *100*, 7566.
(37) Lalande, G.; Côté, R.; Guay, D.; Dodelet, J. P.; Weng, L. T.; Bertrand, P. *Electrochim. Acta* **1997**, *42*, 1379.
(38) Fournier, J.; Lalande, G.; Côté, R.; Guay, D.; Dodelet, J. P. *J. Electrochem. Soc.* **1997**, *144*, 218.
(39) Côté, R.; Lalande, G.; Guay, D.; Dodelet, J. P.; Dénès, G. *J. Electrochem. Soc.* **1998**, *145*, 2411.
(40) Côté, R.; Lalande, G.; Faubert, G.; Guay, D.; Dodelet, J. P.; Dénès, G. *J. New Mater. Electrochem. Syst.* **1998**, *1*, 7.
(41) Faubert, G.; Côté, R.; Guay, D.; Dodelet, J. P.; Dénès, G.; Poleunis, C.; Bertrand, P. *Electrochim. Acta* **1998**, *43*, 1969.
(42) Wang, H.; Côté, R.; Faubert, G.; Guay, D.; Dodelet, J. P. *J. Phys. Chem. B* **1999**, *103*, 2042.
(43) Bouwkamp-Wijnoltz, A. L.; Visscher, W.; van Veen, J. A. R.; Tang, S. C. *Electrochim. Acta* **1999**, *45*, 379.
(44) Wei, G.; Wainright, J. S.; Savinell, R. F. *J. New Mater. Electrochem. Syst.* **2000**, *3*, 121.
(45) Bron, M.; Fiechter, S.; Hilgendorff, M.; Bogdanoff, P. *J. Appl. Electrochem.* **2002**, *32*, 211.
(46) Faubert, G.; Côté, R.; Dodelet, J. P.; Lefèvre, M.; Bertrand, P. *Electrochim. Acta* **1999**, *44*, 2589.
(47) He, P.; Lefèvre, M.; Faubert, G.; Dodelet, J. P. *J. New Mater. Electrochem. Syst.* **1999**, *2*, 243.
(48) Dignard-Bailey, L.; Trudeau, M.; Joly, A.; Schulz, R.; Lalande, G.; Guay, D.; Dodelet, J. P. *J. Mater. Res.* **1994**, *9*, 3202.
(49) Lefèvre, M.; Dodelet, J. P.; Bertrand, P. *J. Phys. Chem. B* **2002**, *106*, 8705.
(50) Rouquerol, F.; Rouquerol, J.; Sing, K. *Adsorption by Powders and Porous Solids*; Academic Press: London, 1999; p 444.
(51) Boehm, H. P.; Mair, G.; Stoehr, T.; De Rincon, A. R.; Tereczki, B. *Fuel* **1984**, *63*, 1061.
(52) Stöhr, B.; Boehm, H. P.; Schlögl, R. *Carbon* **1991**, *29*, 707.
(53) Atamny, F.; Blöcker, J.; Dübotzky, A.; Kurt, H.; Timpe, O.; Loose, G.; Mahdi, W.; Schlögl, R. *Mol. Phys.* **1992**, *76*, 851.
(54) Kinoshita, K. In *Carbon, Electrochemical and Physicochemical Properties*; John Wiley & Sons: New York, 1988; p 295.
(55) Sepa, D. B.; Vojnovic, M. V.; Damjanovic, A. *Electrochim. Acta* **1981**, *26*, 781.
(56) Sepa, D. B.; Vojnovic, M. V.; Vracar, L. M. *Electrochim. Acta* **1984**, *29*, 1169.
(57) Damjanovic, A.; Sepa, D. B.; Vojvonic, M. V. *Electrochim. Acta* **1979**, *24*, 887.
(58) Parthasarathy, A.; Martin, C. R.; Srinivasan, S. *J. Electrochem. Soc.* **1991**, *138*, 916.
(59) Beattie, P. D.; Basura, V. I.; Holdcroft, S. *J. Electroanal. Chem.* **1999**, *468*, 180.
(60) McDonald, D. D. In *Transient Techniques in Electrochemistry*; Plenum Press: New York, 1977; p 191.
(61) Pels, J. R.; Kapteijn, F.; Moulijn, J. A.; Zhu, Q.; Thomas, K. M. *Carbon* **1995**, *33*, 1641.
(62) Casanovas, J.; Manel Ricart, J.; Rubio, J.; Illas, F.; Jiménez Mateos, J. M. *J. Am. Chem. Soc.* **1996**, *118*, 8701.
(63) Fierro, J. L. G. *Surf. Interface Anal.* **1996**, *24*, 223.
(64) Luk'yanov, I. M.; Shchukarev, A. V.; Smirnov, E. P.; Aleskovskii, V. B. *Theor. Exp. Chem.* **1989**, *25*, 454.
(65) Moulder, J. F.; Stickle, W. F.; Sobol, P. E.; Bomben, K. D. In *Handbook of X-ray Photoelectron Spectroscopy*, Chastain, J., Ed.; Perkin-Elmer Corporation: Eden Prairie, MN 1992; p 253.
(66) Xie, Y.; Sherwood, P. M. A. *Chem. Mater.* **1990**, *2*, 293.
(67) Choudury, T.; Saied, S. O.; Sullivan, J. L.; Abbot, A. M. *J. Phys. D: Appl. Phys.* **1989**, *22*, 1185.
(68) Sethuraman, A. R.; Stencel, J. M.; Rubel, A. M.; Cavin, B.; Hubbard, C. R. *J. Vac. Sci. Technol.* **1994**, *A12*, 443.
(69) Reinartz, C.; Fürbeth, W.; Stratmann, M. Fresenius *J. Anal. Chem.* **1995**, *353*, 657.